JACS
JOURNAL OF THE AMERICAN CHEMICAL SOCIETY

Article

pubs.acs.org/JACS

Molecular View of Phase Coexistence in Lipid Monolayers

Svetlana Baoukina, Eduardo Mendez-Villuendas, and D. Peter Tieleman*

Department of Biological Sciences and Institute for Biocomplexity and Informatics, University of Calgary, 2500 University Drive NW, Calgary, AB, Canada T2N 1N4

ABSTRACT: We used computer simulations to study the effect of phase separation on the properties of lipid monolayers. This is important for understanding the lipid–lipid interactions underlying lateral heterogeneity (rafts) in biological membranes and the role of domains in the regulation of surface tension by lung surfactant. Molecular dynamics simulations with the coarse-grained MARTINI force field were employed to model large length (~80 nm in lateral dimension) and time (tens of microseconds) scales. Lipid mixtures containing saturated and unsaturated lipids and cholesterol were investigated under varying surface tension and temperature. We reproduced compositional lipid demixing and the coexistence of liquid-expanded and liquid-condensed phases as well as liquid-ordered and liquid-disordered phases. Formation of the more ordered phase was induced by lowering the surface tension or temperature. Phase transformations occurred via either nucleation or spinodal decomposition. In nucleation, multiple domains formed initially and subsequently merged. Using cluster analysis combined with Voronoi tessellation, we characterized the partial areas of the lipids in each phase, the phase composition, the boundary length, and the line tension under varying surface tension. We calculated the growth exponents for nucleation and spinodal decomposition using a dynamical scaling hypothesis. At low surface tensions, liquid-ordered domains manifest spontaneous curvature. Lateral diffusion of lipids is significantly slower in the more ordered phase, as expected. The presence of domains increased the monolayer surface viscosity, in particular as a result of domain reorganization under shear.

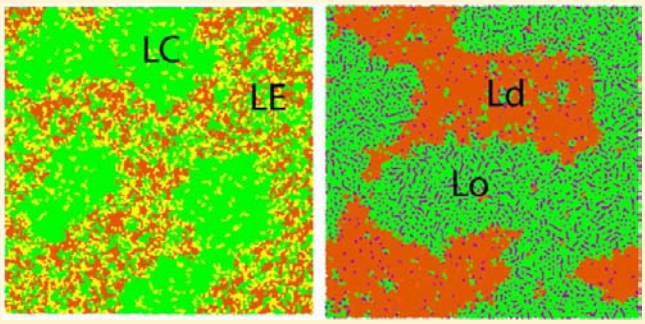

INTRODUCTION

Biological membranes contain multiple lipid species that are organized laterally into regions with distinct properties—domains of coexisting phases.[1−3] Lateral organization of lipids serves to optimize the environment for biochemical reactions.[4] In cell membranes, the raft hypothesis suggests the presence of nanoscale dynamic domains of a liquid-ordered-like phase enriched in cholesterol and sphingomyelin and incorporating specific proteins.[5] Rafts are important in membrane trafficking, signal transduction (including immune response), and entry and budding of pathogens.[6−10] Lateral organization of lipids also plays an important role by modulating the membrane structure and properties. In lung surfactant, a monolayer lining the gas exchange interface in the lungs, saturated and unsaturated lipids are separated into coexisting phases.[11−13] Squeeze-out and reincorporation of liquid-expanded domains enriched in unsaturated lipids provides low surface tensions during the breathing cycle.[14,15]

Because of their importance, domains in biological membranes have attracted growing scientific interest.[16] Despite extensive studies, the nature of domains, in particular on the nanometer scale, remains controversial.[17−20] In lung surfactant, the structure of more ordered domains (liquid-condensed vs liquid-ordered phases) and their role in surface activity are not fully understood. Rafts have been observed only indirectly in vivo and differ in size and life span. In contrast to in vivo dynamic nanoscale rafts, model membranes (bilayers) containing raft-forming lipids show persistent macroscopic phase separation. Current theories offer various explanations for this discrepancy, including active cellular processes (lipid transport and recycling), lipid–protein interactions, adhesion to cytoskeleton (protein fences), protein scaffolds, and specific lipid–lipid interactions (see, e.g., refs 17, 18, and 21 for reviews).

Lipid–lipid interactions alone could produce nanoscale domains via different theoretical scenarios. In a single-phase region, the vicinity to a critical point gives rise to transient compositional fluctuations. The characteristic size of "domains" is then given by the correlation length, which diverges as the critical point is approached.[22,23] Coupling between leaflets with asymmetric composition can induce or suppress phase separation.[24,25] Rafts could also represent a microemulsion driven by coupling of curvature to compositional differences between the leaflets.[26]

Within a phase-coexistence region, several factors can prevent coagulation and stabilize small domains. At low line tensions at the domain boundaries, a large number of small domains becomes favorable because of the resulting entropy gain. Line tension arises from hydrophobic mismatch and

Received: May 17, 2012
Published: September 24, 2012

   dx.doi.org/10.1021/ja304792p | J. Am. Chem. Soc. 2012, 134, 17543−17553

difference in chain order between the two phases and could be lowered by lipids containing a saturated chain and an unsaturated chain.[27,28] Long-range repulsive forces also favor a small domain size. Repulsion can originate from spontaneous curvature of domains[29,30] or from uncompensated out-of-plane electrostatic dipole moments,[31,32] such as in lipid monolayers.

Distinguishing among the large number of theories of domain formation in biological membranes remains elusive because their experimental verification is challenging.[20,33] This is due to difficulties in obtaining experimental data at both high spatial and temporal resolutions. Over the past decade, the range of problems accessible in typical computer simulations has advanced significantly, from a small lipid patch or protein fragment on nanosecond time scales to complex protein−lipid assemblies on time scales of tens of microseconds.

Here we used molecular dynamics (MD) simulations with the coarse-grained (CG) MARTINI force field[34] to model monolayers at large length (80 nm in lateral dimension) and time (tens of microseconds) scales while retaining a significant amount of molecular detail. We focused on phase separation in lipid monolayers as a step towards understanding lipid−lipid interactions underlying lateral heterogeneity in biological membranes. Lipid monolayers allow varying molecular areas over several phases, are convenient to study experimentally, are often used as model systems for cell membranes, and are directly relevant for studying lung surfactant.

Previous MD studies using both atomistic and CG force fields have simulated phase transformations in lipid bilayers and monolayers.[35−40] However, only a small number of studies have investigated phase coexistence, and they were generally limited to small time and length scales because of computational limits. In lipid monolayers, the coexistence of liquid-condensed (LC) and liquid-expanded (LE) phases was earlier simulated using the MARTINI model,[41,42] with mainly qualitative analysis of the domain properties. In lipid bilayers, compositional demixing of long- and short-chain lipids (having high and low melting temperatures, respectively) and coexistence of the gel and liquid-crystalline (Lα) phases were simulated with CG models.[43−45] The phase coexistence of liquid-ordered (Lo) and liquid disordered (Ld) phases was reproduced in raft-forming lipid mixtures using the MARTINI model.[46−50] In those studies, the compositions of the phases, their thicknesses, order parameters, lipid mobilities, and the line tension at the phase boundary were characterized.

In this work, we reproduced two physiologically relevant cases: the coexistence of LE and LC phases (Figure 1) and of Lo and Ld phases (Figure 2), which at certain surface densities/surface tensions show strong similarities to Lα and gel phases and Lo and Ld phases in bilayers, respectively. Compositional lipid demixing was induced in ternary mixtures of saturated and unsaturated lipids and cholesterol under varying surface tension and temperature. By employing cluster analysis with Voronoi tessellation (Figure 3), we obtained detailed information on a number of domain properties, including the surface-tension-dependent composition, partial lipid areas, boundary length, and fraction of each phase. In contrast to previous studies, the large monolayer size in this work (~10 000 lipids per monolayer) allowed the formation of multiple domains, enabling us to analyze their independent growth and merging while retaining near-atomic resolution. We observed phase separation by two mechanisms, nucleation and spinodal decomposition, with distinct domain morphology and kinetics of growth. Our study provides a molecular view of liquid−liquid and liquid−solid phase coexistence in lipid membranes on length scales detectable using emerging experimental methods such as super-resolution microscopy.[51−53]

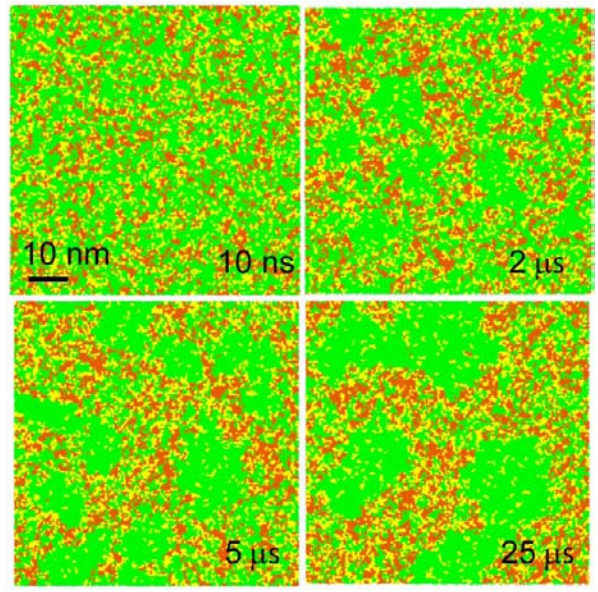

Figure 1. Formation of LC domains in the LE phase in a 3:1:1 DPPC:POPG:DOPC mixture at a surface tension of 5 mN/m at 290 K. Top view; DPPC is shown in green, POPG in yellow, and DOPC in orange; water is not shown.

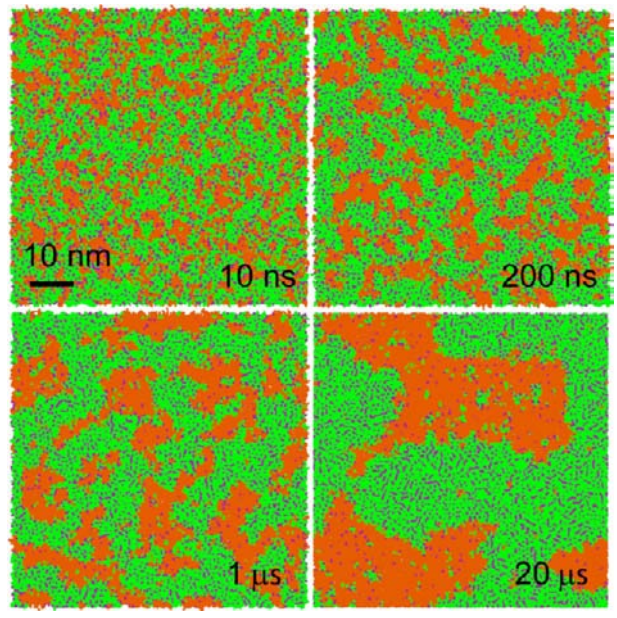

Figure 2. Phase separation into Lo and Ld phases in a 5:3:4 DPPC:DOPC:cholesterol mixture at a surface tension of 30 mN/m at 290 K. View as in Figure 1; DPPC is shown in green, DOPC in orange, and cholesterol in purple.

METHODS

Simulations were performed using the GROMACS software package (version 4).[54] The mixtures of saturated and unsaturated lipids and cholesterol were studied under varying surface tension (1−30 mN/m) and temperature (270−323 K) to reproduce transformations between either the LE and LC phases or the Lo and Ld phases. A summary of the simulations is given in Table 1.

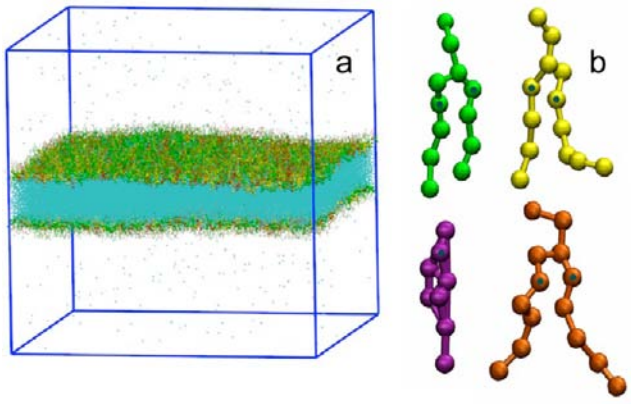

Figure 3. (a) System setup and (b) lipids in the MARTINI model. Color scheme: DPPC in green, POPG in yellow, DOPC in orange, cholesterol in purple; water in cyan, simulation box edges in dark blue.

The system setup consisted of a water slab in vacuum with two symmetric monolayers at the two water−vacuum interfaces (Figure 3a). The monolayers consisted of dipalmitoylphosphatidylcholine (DPPC), dioleoylphosphatidylcholine (DOPC), palmitoyloleoylphosphatidylglycerol (POPG), and cholesterol. We selected the lipid ratios 3:1:1 DPPC:POPG:DOPC and 5:3:4 DPPC:DOPC:cholesterol, which are called in the text the LC/LE and Lo/Ld mixtures, respectively. The lipids were randomly mixed in the starting configuration, and then the target surface tension and temperature were applied.

We simulated small and large membrane patches of 2304 and 9216 lipids per monolayer, corresponding to box lateral sizes of ∼40 and ∼80 nm, respectively. Depending on the lipid composition, the water slab contained ∼60 000 and ∼350 000 water particles for the small and large monolayers, respectively; Na^+ ions were added to neutralize the charge of anionic POPG lipids.

We used the MARTINI CG force field.[34] In this force field, molecules are represented by particles that group approximately four heavy atoms together (Figure 3b). DPPC and DOPC are standard components of this force field. For POPG, the glycerol group in the headgroup was represented by a polar particle, P4, as in previous simulations.[55,56] In the unsaturated hydrocarbon chains, the particle type at sites D3A,B and C4A,B was changed to C4, analogous to the raft-forming lipid mixture in ref 46; the angle potential at these sites was also modified to an equilibrium angle of 100° and a force constant of 10 kJ mol^{-1} rad^{-2} to reproduce a decrease in the order parameter profile at the unsaturated bond.

For nonbonded interactions, the standard cutoffs for the MARTINI force field were used: the Lennard-Jones potential was shifted to zero between 0.9 and 1.2 nm, and the Coulomb potential was shifted to zero between 0 and 1.2 nm with a relative dielectric constant of 15. The time step was 20 fs, and the neighbor list was updated every 10 steps. Lipids and water were coupled separately to a target temperature using the velocity rescaling thermostat[57] with a time constant of 1 ps. A target surface tension was maintained using the surface tension coupling scheme and the Berendsen barostat[58] with a time constant of 4 ps and a compressibility of 5×10^{-5} bar^{-1} in the lateral direction; the compressibility in the normal direction was set to zero to prevent box contraction. The simulation time was 25 μs for simulations in which phase separation occurred and 5 μs for homogeneous membranes. The actual simulation time is indicated everywhere in the text. Thermodynamic properties were calculated by averaging over the last microsecond of the trajectory. Diffusion coefficients were calculated from the last 500 ns of the trajectory after subtracting the center-of-mass motion of the monolayers. The kinetics of domain growth was characterized over the whole trajectory.

Table 1. Summary of Simulations Performed[a]

C	N	T (K)	γ_m (mN/m)	t (μs)	phase
3:1:1 DPPC:POPG:DOPC	2304	310	30	5	LE
			20	5	LE
			10	5	LE
			5	5	LE
		290	30	5	LE
			20	5	LE
			10	5	LE
			7	25	LE + LC
			5	25	LE + LC
			1	25	LE + LC
	9216	290	10	5	LE
			7	25	LE + LC
			5	3 × 25	LE + LC
			1	25	LE + LC
5:3:4 DPPC:DOPC:cholesterol	2304	323	30	25	F
			20	25	F
			10	25	F
			5[b]	25	F
		290	30	25	Ld + Lo
			20	25	Ld + Lo
			10	25	Ld + Lo
			5	25	Ld + Lo
	9216	290	30	2 × 25	Ld + Lo
			5	2 × 25	Ld + Lo

[a]Here C is the monolayer composition, N is the number of lipids per monolayer, T is the absolute temperature, γ_m is the surface tension, and t is the simulation time; LE denotes the liquid-expanded phase, LC the liquid-condensed phase, Lo the liquid-ordered phase, Ld the liquid-disordered phase, and F compositional fluctuations. [b]This monolayer was unstable and collapsed after ∼13 μs. The monolayer structure before collapse was characterized for the purpose of comparison.

To characterize the kinetics of domain growth, we performed two additional independent simulations of the large monolayers for each composition (see Table 1). The later stages of coarsening, where the domain sizes became comparable to the box size and led to strong deviations in the average domain size, were excluded from the analysis of the growth kinetics.

We also performed controls on the small monolayers for both mixtures at 5 mN/m and 290 K using a dissipative particle dynamics (DPD)-like thermostat with pairwise impulsive friction as described in ref 59, with isotropic friction at a rate of 1 ps^{-1}. This thermostat uses Galilean-invariant relative frictions, which provide conservation of linear momentum and maintain the correct dynamics in the limit of large length and time scales.

Because of the strong lateral heterogeneity, we did not directly calculate the monolayer thickness. The chain order parameter, S_z, was calculated using the formula

$$S_{z,n} = \left\langle \frac{1}{2}(3\cos^2\theta_n - 1) \right\rangle$$

where θ_n is the angle between the vector connecting the $n-1$ and $n+1$ sites of the hydrocarbon chain and the monolayer normal z and the average is over all sites (C1 to C5) for both chains and over all lipids constituting the given phase, except for cholesterol.

The line tension at the domain boundary, λ, was calculated from the pressure tensor components P_{yy} and P_{xx} of stripelike domains oriented along the x axis and periodic in this direction. For this purpose, additional 10 μs simulations were performed for the small monolayers. The following formula was used:

$$\lambda = \frac{1}{4}L_y L_z (P_{yy} - P_{xx})$$

where L_y and L_z are the y and z dimensions of the box and the factor of $^1/_4$ accounts for the total of four boundaries in the two monolayers.

The monolayer surface viscosity, η_m, which approximately represents a three-dimensional (3D) viscosity multiplied by a monolayer thickness, was calculated using the formula[60]

$$\eta_m = \frac{1}{2s}[P_{xy}(s)L_z - \eta_w s L_w]$$

where η_w is the viscosity of water [$(7.7 \pm 0.4) \times 10^{-4}$ Pa s, as calculated in ref 56], L_w is the thickness of the water slab in the simulations, and s is the shear rate. To calculate η_m, additional 10 μs shear-flow simulations at two shear rates were performed for the small monolayers (see Table 3).

We developed a MATLAB (version R2011b)-based program to perform quantitative analysis of the domains (Figure 4) [Mendez-Villuendas et al., in preparation]. The area occupied by each lipid was calculated on the basis of Voronoi tessellation. The C1A,B sites in DPPC, POPG, and DOPC and the R1 site in cholesterol (indicated as dots in Figure 3b) were selected as the centers of Voronoi polygons. These sites were then distributed between the two coexisting phases using cluster analysis based on a connectivity matrix with a selected cutoff, R_{cut}. The cutoff corresponded roughly to the square root of the inverse average density of the Voronoi sites. In addition, lipids belonging to a more ordered phase were required to have an average chain order parameter, S_z, larger than a selected cutoff. To distinguish between compositional fluctuations and actual domains of the new phase, a cutoff on the domain size, N_{cut}, was also introduced. These numbers were chosen by monitoring the fraction of small clusters constantly present on the simulation time scale. The following cutoff values were used for the two lipid mixtures: R_{cut} = 0.55 nm, S_z = 0.4, and N_{cut} = 100 sites for the coexisting LC/LE mixture (as the LC phase is nearly incompressible in the selected narrow surface tension interval) and R_{cut} = 0.550−0.592 nm, S_z = 0.3, and N_{cut} = 10 sites for the Lo/Ld mixture.

The average domain size, R, was calculated from the average domain area, $\langle A \rangle$, using the expression $R = (\langle A \rangle/\pi)^{1/2}$. The size of the critical nucleus was determined from the cluster analysis as the largest compositional fluctuation that did not lead to domain growth. To improve the statistics for this particular property, four additional 1 μs simulations were performed for the 3:1:1 DPPC:POPG:DOPC mixture at 5 mN/m and 290 K, to give a total of 10 data sets. The apparent nucleation rate, $\dot{N}$, was calculated from the time dependence of N', the number of clusters larger than the critical nucleus:

$$\dot{N} = \frac{1}{A_0}\frac{dN'}{dt}$$

where A_0 is monolayer area.

The monolayer curvature was characterized using a second MATLAB (v.R2011b)-based program [Mendez-Villuendas et al., in preparation]. The phosphate groups of lipids (PO4 sites) were fitted to a surface using a two-dimensional (2D) binomial filter with a 6 nm characteristic length to remove the noise. The resulting convoluted surface was then converted to an equally spaced grid (0.6 nm), for which partial derivatives were calculated to find the principal curvatures c_1 and c_2 and the mean curvature $H = (c_1 + c_2)/2$.

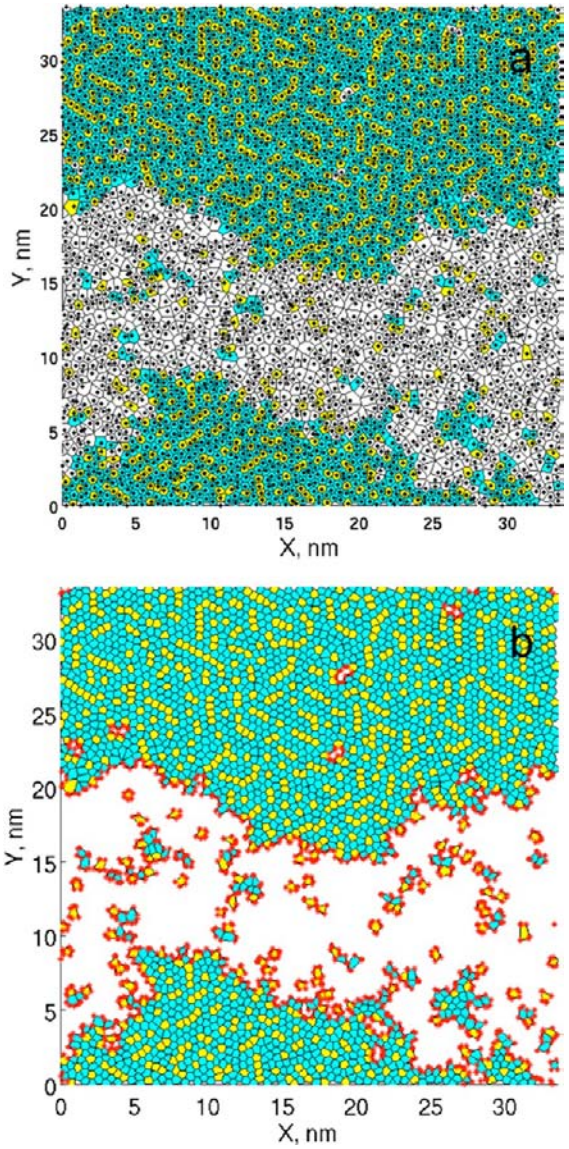

Figure 4. Cluster analysis based on Voronoi tessellation using C1A, C1B, and R1 particles as centers for Voronoi polygons. (a) Polygons corresponding to DPPC and cholesterol forming the Lo phase are colored in green and yellow, respectively. (b) The phase boundary is shown in red.

dx.doi.org/10.1021/ja304792p | J. Am. Chem. Soc. 2012, 134, 17543−17553

RESULTS

Isotherms. For the simulated lipid mixtures, we first calculated the surface tension−area isotherms (Figure 5). The

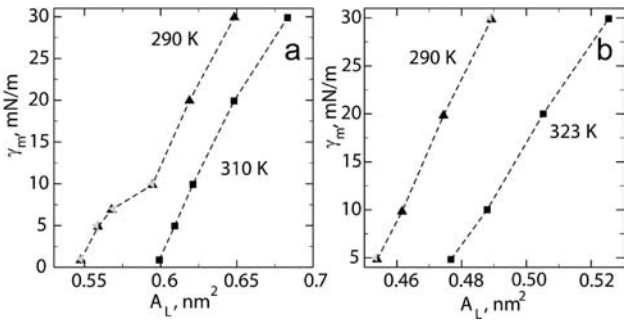

Figure 5. Surface tension−area isotherms calculated for the (a) 3:1:1 DPPC:POPG:DOPC and (b) 5:3:4 DPPC:DOPC:cholesterol monolayers. Data points are shown as black triangles and squares for the small monolayers and gray triangles for the large monolayers (points overlap).

surface tension in the monolayer, γ_m, at a given area per lipid, A_L, can be related to the experimentally measured surface pressure, $\Pi(A_L)$, using the standard formula $\gamma_m(A_L) = \gamma_0 - \Pi(A_L)$, where γ_0 is the surface tension at the pure air−water interface. Notably, for both mixtures, the isotherms for the small and large monolayers (see Methods) were essentially the same.

The 3:1:1 DPPC:POPG:DOPC monolayer was roughly homogeneous at 310 K and formed an LE phase. At 290 K, a transformation into an LC phase occurred at low surface tensions, manifested as a plateau on the isotherm. At and below the plateau, coexistence of the LE and LC phases was observed. The LC phase consisted mainly of DPPC lipids with a small fraction of POPG that varied with surface tension (see below).

In the 5:3:4 DPPC:DOPC:cholesterol monolayer, coexistence of the Lo and Ld phases was observed at 290 K within the studied interval of surface tensions. The Lo phase consisted of DPPC and cholesterol arranged into a distorted hexagonal lattice, while the Ld phase was highly enriched in DOPC (Figure 6a). At 323 K, transient large clusters close in composition to the Lo phase (i.e., strong compositional fluctuations) were observed (Figure 6b).

Order of Phases. The coexisting phases were then characterized using the in-plane (2D) radial distribution function (RDF) (Figure 7). Compared with a roughly homogeneous LE phase (Figure 7a), coexistence of the LC

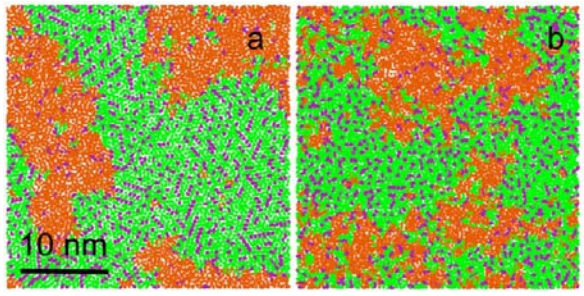

Figure 6. Phase behavior in the 5:3:4 DPPC:DOPC:cholesterol mixture at (a) 290 and (b) 323 K. Top view; color scheme as in Figure 2.

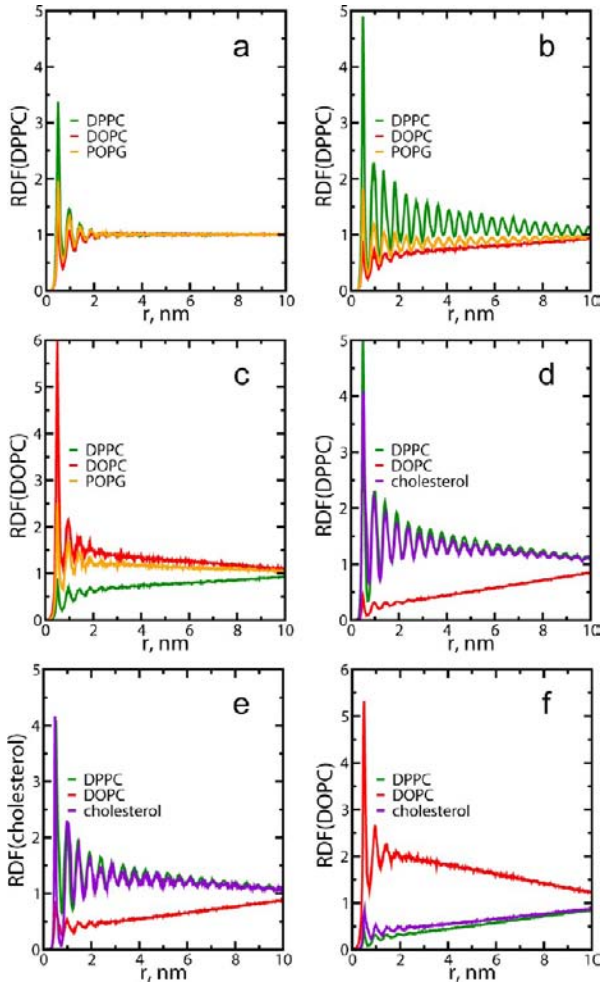

Figure 7. In-plane RDFs for lipids. (a) The 3:1:1 DPPC:POPG:-DOPC monolayer is homogeneous at a surface tension of 5 mN/m at 310 K, and (b, c) it separates into LE and LC phases at a lower temperature of 290 K. (d−f) The 5:3:4 DPPC:DOPC:cholesterol monolayer is separated into Lo and Ld phases at a surface tension of 30 mN/m at 290 K. Color scheme: DPPC in green, POPG in orange, DOPC in red, cholesterol in purple.

and LE phases is visible by long-range translational order and segregation of saturated DPPC in the LC domains (Figure 7b,c). Even stronger compositional demixing was observed for the Lo and Ld phases (Figure 7d−f). The translational order decayed faster in the Lo phase than in the LC phase, consistent with the liquid nature of the former versus the solidlike nature of the latter.

The orientational order of lipid hydrocarbon chains (Table 2) generally increased as the temperature and surface tension decreased. The chain order parameter S_z (see Methods) was slightly larger in the LC phase than in the Lo phase and noticeably larger in the LE phase than in the Ld phase because of the higher concentration of saturated lipids in the former (see below). The calculated order parameters are in good agreement with values previously reported for lipid bilayers and monolayers forming these phases in the MARTINI model.[42,46]

Area per Lipid. In the coexistence region, the area per lipid in each phase (Figure 8) differed from the average area per lipid shown in the isotherms (Figure 5). In the LC/LE mixture, the average area per lipid decreased with decreasing surface tension, while the areas per lipid in the individual phases remained

dx.doi.org/10.1021/ja304792p | J. Am. Chem. Soc. 2012, 134, 17543−17553

Table 2. Orientational Order Parameters and Line Tensions[a]

C	N	T (K)	γ_m (mN/m)	phase	S_z	λ (pN)
3:1:1 DPPC:POPG:DOPC	2304	310	30	LE	0.44	
		290	30	LE	0.50	
			10	LE	0.60	
			7	LE/LC	0.58/0.92	
			5	LE/LC		43
			1	LE/LC		28
5:3:4 DPPC:DOPC:cholesterol[b]	2304	323	30	F (Ld/Lo)[c]	0.29/0.73	
		290	30	Ld/Lo	0.32/0.89	15
			10	Ld/Lo		9
			5	Ld/Lo	0.40/0.89	

[a]Here C is the monolayer composition, N is the number of lipids per monolayer, T is the temperature, and γ_m is the surface tension; LE denotes the liquid-expanded phase, LC the liquid-condensed phase, Lo the liquid-ordered phase, Ld the liquid-disordered phase, and F fluctuations; S_z is the orientational order parameter averaged over all sites representing lipid hydrocarbon chains (C1 through C5), and λ is the line tension at the phase boundary. [b]Cholesterol was not considered in the calculation of S_z. [c]S_z was calculated for the Lo and Ld clusters.

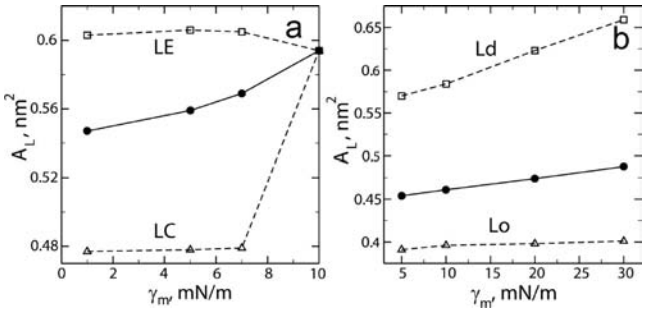

Figure 8. Areas per lipid in the (a) LE and LC and (b) Lo and Ld coexisting phases at 290 K. Solid lines correspond to the average areas per lipid in the monolayers as shown in Figure 5.

nearly constant (Figure 8a). In the Lo/Ld mixture, the areas per lipid decreased with decreasing surface tension, particularly in the Ld phase (Figure 8b). The values for the Lo phase are in agreement with experimental studies on lipid monolayers[61] and with previous simulation results for lipid bilayers.[46]

The partial area of DPPC lipid in the Lo phase at 290 K (Figure 9a) was close to but slightly higher than that in the LC

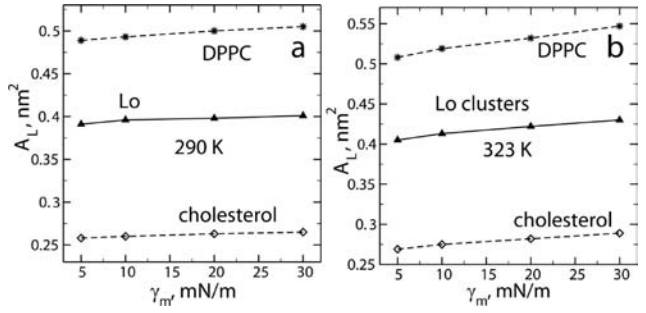

Figure 9. Partial areas per DPPC and cholesterol in the Lo phase at (a) 290 and (b) 323 K.

phase (compare to, e.g., the areas in DPPC monolayers in refs 41 and 42) because of the condensing effect of cholesterol, in agreement with theoretical predictions (see, e.g., refs 62 and 63 and references therein). The partial DPPC area in the Lo clusters at 323 K was larger (Figure 8b) and became similar to the area in an LE phase at higher surface tensions. This change in DPPC partial area with temperature supports the difference in phase behavior (domains vs fluctuations) mentioned above.

Composition. In the LC/LE mixture, the composition of each phase depends on the surface tension. The fraction of DPPC lipids forming the LC phase (Figure 10a) and the total

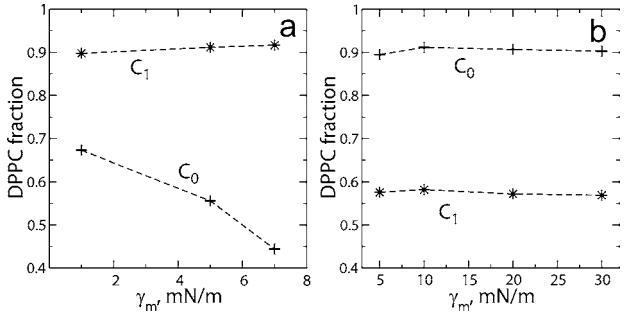

Figure 10. Concentration of DPPC lipids in the (a) LC and (b) Lo phases. C_0 is the DPPC fraction forming the ordered phase (Lo or gel), and C_1 is the DPPC composition of the ordered domains.

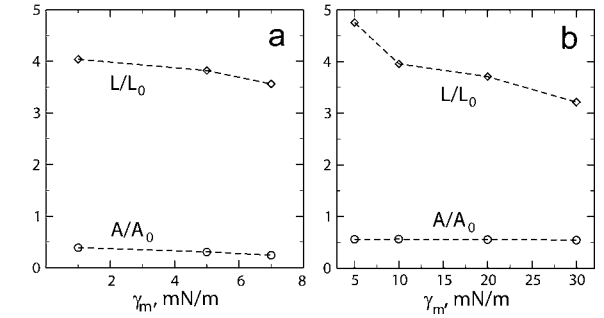

Figure 11. Area fraction, A/A_0, and normalized boundary length, L/L_0, of the (a) LC and (b) Lo phases. The areas A are normalized to the area of the simulation box, A_0; the boundary lengths are normalized to L_0, the perimeter corresponding to a single circular domain with area A.

fraction of LC phase (Figure 11a) increased as the surface tension decreased. At the same time, the relative proportion of DPPC in the LC phase decreased as more POPG lipids were condensed by monolayer lateral compression. POPG contains one saturated and one unsaturated chain and is a likely candidate for a line-active lipid.[27] However, we did not observe its segregation or enrichment at the phase boundary, although

dx.doi.org/10.1021/ja304792p | J. Am. Chem. Soc. 2012, 134, 17543−17553

Table 3. Diffusion and Surface Viscosity[a]

C	N	T (K)	γ_m (mN/m)	phase	D (10^{-7}cm^2/s)	η_m(10^{-10}Pa m s)	
						10^7 s^{-1}	10^6 s^{-1}
3:1:1 DPPC:POPG:DOPC	2304	310	30	LE	20		
		290	30	LE	10	0.1	0.1
			10	LE	8	0.2	0.2
			7	LE/LC	6/0.3		
			5	LE/LC	6/0.2	0.4	0.4
			1	LE/LC	5/0.2		
5:3:4 DPPC:DOPC:cholesterol	2304	323	30	F	9		
		290	30	Ld/Lo	6/0.1	1−0.5	8−0.5
			5	Ld/Lo	2/0.03	3−0.7	10−1

[a]Here C is the monolayer composition, N is the number of lipids per monolayer, T is the temperature, and γ_m is the surface tension; LE denotes the liquid-expanded phase, LC the liquid-condensed phase, Lo the liquid-ordered phase, and Ld the liquid-disordered phase; D is the long-time lateral diffusion coefficient; η_m is the monolayer surface viscosity, values of which are given at two shear rates (values separated by dash are before and after domain reorganization; see the text for details).

this may be because POPG is charged as well as for other reasons.

In the Lo/Ld mixture, the compositions of the phases as well as their fractions varied slightly with surface tension (see Figures 10b and 11b). Most DPPC lipids partitioned into the Lo phase at a 23:17 ratio with cholesterol (Figure 10b). The composition of the Lo phase was in good agreement with that of lipid bilayers from experimental data[64] and simulations with the MARTINI model.[46]

Phase Boundary. The boundary length between the coexisting phases increased with decreasing surface tension (Figure 11). This can be explained by a decrease in line tension (Table 2). The latter is likely caused by a decrease in the hydrophobic mismatch between the ordered (thicker) and disordered (thinner) phases upon monolayer compression. In the Ld phase, the area per lipid decreased (Figure 8b), which in turn increased the thickness. In the LE phase, the fraction of DOPC lipids increased (Figure 10a), while the area per lipid did not change noticeably (Figure 8a). Given a higher area per lipid of DOPC compared with DPPC,[65,66] this in turn produced an increase in thickness.

The calculated values for the line tensions are approximately an order of magnitude higher than experimental values for lipid bilayers and monolayers.[29,67−70] However, the line tension in monolayers was typically measured at much higher surface tensions. In addition, the difference in scales for domain boundary measurements (μm in experiments vs Å in simulations), leading to different levels of detail, could play a role. Previous simulations with the MARTINI model reported a value of 3.5 pN per leaflet for the Lo−Ld interface in bilayers.[46] Recent simulations based on longer time scales reported larger values for bilayers of 14−20 pN,[48,71] which are comparable to the results of our study.

Dynamic Properties. Lipid long-time lateral diffusion (Table 3) became slower as the temperature and surface tension decreased, as expected. The transition to a more ordered phase was accompanied by a decrease in the diffusion coefficient (D) by 1−2 orders of magnitude, consistent with the results of experimental studies[72−75] and previous simulations with the MARTINI model.[36,42,46] Here, somewhat faster diffusion was observed in the LC phase, which could be related to the small size of the LC domains. Even slower diffusion in the Lo phase at 5 mN/m and 290 K could be associated with its higher density or nonflat character (Figure 12). Domains of the Lo phase have a negative spontaneous curvature (approximately −0.06 nm^{-1}), likely induced by cholesterol.[76]

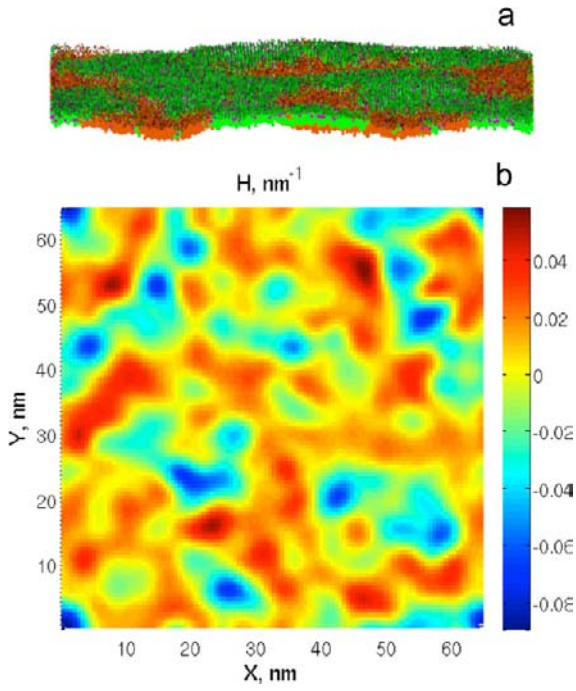

Figure 12. Monolayer of 5:3:4 DPPC:DOPC:cholesterol at a surface tension of 5 mN/m at 290 K. (a) Side view, with lipid headgroups shown as spheres, tails shown as sticks, and water not shown; color scheme as in Figure 2. (b) Mean curvature surface.

The monolayer surface viscosities, η_m (Table 3), were in agreement with the results of previous simulations[56,60] and lower than the experimental values,[77,78] while the shear rates accessible in simulations were much higher than the experimental ones ($\lesssim 10^1$ s^{-1}). Monolayer lateral compression generally led to higher surface viscosities. Formation of the LC domains further increased the viscosity, in agreement with experimental findings.[79] Interestingly, this increase occurred at an unchanged area per lipid in the LE phase (see Figure 8a) and a higher fraction of unsaturated lipid in the LE phase, which would reduce the viscosity in the absence of LC domains.[78] Shear deformations caused rotation of the LC domains but did not perturb their structure. In monolayers with

dx.doi.org/10.1021/ja304792p | J. Am. Chem. Soc. 2012, 134, 17543−17553

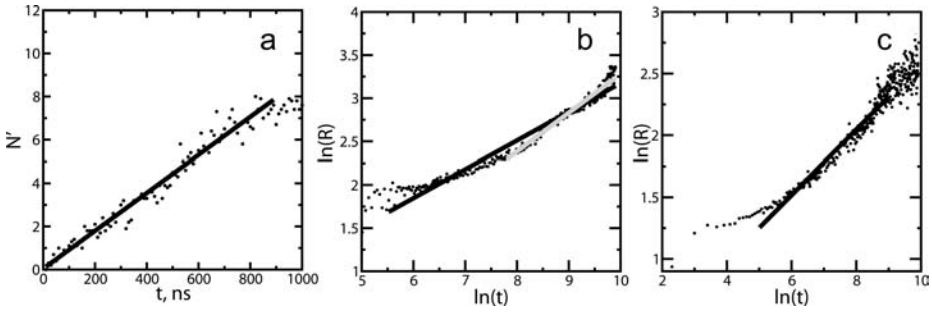

Figure 13. Nucleation and growth of domains. (a) Number of clusters larger than the critical nucleus vs time and (b, c) average domain size vs time on a logarithmic scale for the (a, b) 3:1:1 DPPC:POPG:DOPC and (c) 5:3:4 DPPC:DOPC:cholesterol monolayers at 5 mN/m and 290 K. Solid lines show linear fits.

Table 4. Kinetics of Domain Growth[a]

C	N	T (K)	γ_m (mN/m)	thermostat	phase	α	correlation coefficient
3:1:1 DPPC:POPG:DOPC	2304	290	5	DPD-like	LC/LE	0.33	0.94
				v-rescale		0.33	0.94
	9216	290	5	v-rescale	LC/LE	0.33; 0.45[b]	0.98
5:3:4 DPPC:DOPC:cholesterol	2304	290	5	DPD-like	Lo/Ld	0.26	0.95
				v-rescale		0.25	0.93
	9216	290	30	v-rescale	Lo/Ld	0.26	0.98
			5			0.26	0.98

[a]Here C is the monolayer composition, N is the number of lipids per monolayer, T is the temperature, γ_m is the surface tension, and α is the growth exponent. [b]Obtained from a fit at later times ($t > 2$ μs). In large monolayers, fitting was performed on averages over six and four independent trajectories for the LC/LE and Lo/Ld mixtures, respectively. See the text for details.

coexisting Lo/Ld phases, the monolayer underwent reorganization under shear flow: its morphology changed from a continuous network to stripes along the direction of shear. Because of this reorganization (which took ~1 μs and ~100 ns, at the lower and higher rates, respectively), the viscosity noticeably decreased with time.

Mechanism of Phase Transformation. The mechanism of phase transformation differed for the two different lipid mixtures. In the first mixture, formation of the LC phase from the LE phase proceeded via nucleation and growth. This transformation was initiated by local compositional fluctuations approaching the properties of the LC phase. The transformation was characterized by an energy barrier; fluctuations larger than a critical nucleus continued to grow. A thus-formed LC domain in the LE matrix had a dropletlike morphology. Multiple domains formed initially and consequently merged.

In the second mixture, the transformation into the Ld and Lo phases proceeded via spinodal decomposition. Phase separation in this case had no energy barrier; small compositional fluctuations led to a spontaneous, uniform transformation spread over the entire monolayer. This resulted in a continuous network of domains growing in width. The domain morphology did not change on the simulation time scale.

Nucleation. For the first mixture separating into the LE and LC phases, we also analyzed the nucleation process (see Methods). The size of the critical nucleus at 5 mN/m and 290 K was determined to be ~70 lipids, corresponding to a cluster with a radius of ~3.3 nm. Because of the large fraction of DPPC in the mixture, some nuclei of the LC phase in the form of large DPPC clusters were present before the transformation started; other nuclei appeared during the transformation. The apparent nucleation rate was nearly constant (Figure 13a) and had a value of $\sim 2 \times 10^{-6}$ ns^{-1} nm^{-2}.

Kinetics of Domain Growth. Domain growth or coarsening in our simulations covered more than an order of magnitude in time and length scales and preserved the domain morphology. To analyze the kinetics of coarsening, we applied a dynamical scaling hypothesis[80] suggesting that the time evolution is determined by a single characteristic length, the average domain size R, which changes with time, t, with a characteristic growth exponent α: $R \sim t^{\alpha}$.

The kinetics of phase transformations has been described previously by a number of theories (see refs 80−82 and references therein). The behavior of a large number of systems can be grouped into universality classes determined mainly by the presence of conservation laws and the order parameters, with defined values for the growth exponents. For example, the universality classes of models A and B, corresponding to nonconserved and conserved scalar order parameters, have growth exponents of $^1/_2$ and $^1/_3$, respectively. In monolayers, the number of lipids and lipid composition are conserved properties, while the lipid states are not conserved. This case can be related to model C, which involves an ordering nonconserved field coupled to a nonordering conserved field,[83] depending on the contribution of lipid demixing.[84] However, hydrodynamics also plays an important role.[85] Different mechanisms, including diffusive, viscous, and inertial effects, can dominate at different scales and determine the growth exponent, which also depends on the dimensionality.

Lipid monolayers represent thin liquid-crystalline films with in-plane fluidlike behavior coupled to a 3D solvent. We calculated several hydrodynamic parameters affecting the kinetics of domain coarsening.[86,87] The hydrodynamic length, L_H, given by the ratio of the membrane surface viscosity, η_m, and the bulk viscosity of the solvent, η_w, separates the 2D and 3D growth regimes. In our simulations, $L_H \approx 50$ nm, which is smaller than the experimental values because of the lower η_m in

dx.doi.org/10.1021/ja304792p | J. Am. Chem. Soc. 2012, 134, 17543−17553

our simulations. We expect a quasi-2D growth regime dominated by the membrane flow for $R < L_H$, whereas for $R \approx L_H$ the growth regime is intermediate between 2D and 3D, altering the dynamics. The Reynolds number, Re, determines the ratio of inertial and viscous flows; in our simulations, $Re \sim 10^{-4}$. The Péclet number, $Pe = vL/D$, gives the ratio of advective to diffusive transport. Using the estimates $v = dR/dt$ for the velocity and $L = R$ for the characteristic length, we obtain $Pe \sim 1$.

We then performed controls on the small monolayers using a DPD-like thermostat with pairwise impulsive friction[59] providing conservation of linear momentum (see Methods for details). The calculated growth exponents were almost equal to the values for the small monolayers under the same conditions using the standard simulation parameters (Table 4). Differences in hydrodynamic behavior leading to distinct kinetics would likely play a role on time and length scales that are much larger than the ones in our simulations.

The calculated growth exponents for the large monolayers are presented in Table 4, and the $R(t)$ dependences are shown in Figure 13b,c. In the LC/LE mixture with droplet-shape domains, fitting the entire curve for both small and large monolayers gave an exponent of $\sim^1/_3$. At later stages for the large monolayers, we found a crossover to $\alpha \approx {}^1/_2$ that was not observed for the small monolayers. In the Lo/Ld mixture, which underwent spinodal decomposition with networklike domains, the growth exponent was $\sim^1/_4$ for both the small and large monolayers.

For spinodal decomposition with networklike interconnected domains, the initial stages of growth in binary fluids can be characterized by the interface diffusion mechanism with exponents of ${}^1/_3$ in 3D and ${}^1/_2$ in 2D, followed by a crossover to a viscous regime with $\alpha \approx 1$ in 3D.[88,89] Previous theoretical membrane studies at low Re for elongated domains have reported apparent exponents of ∼0.25 at $Pe \approx 10$ in 2D and ∼0.5 at $Pe \approx 1$ at finite L_H.[86] Different theoretical studies have found an exponent of ${}^1/_2$ in the 3D viscous regime.[87,90] A similar result was also reported in DPD simulations.[91] Lattice-based Monte Carlo simulations, in contrast, reported a value of ${}^1/_4$.[84]

For the dropletlike morphology, Ostwald ripening (evaporation−condensation) is characterized by an exponent of ${}^1/_3$ in 2D and 3D.[92,93] Competing growth by Brownian coagulation[94] (domain diffusion and merging) gives exponents of ${}^1/_2$ in 2D and ${}^1/_3$ in 3D. The growth exponent was previously shown to change from ${}^1/_2$ to ${}^1/_3$ for dropletlike domains upon addition of solvent in DPD simulations[95] and in moving from the 2D regime to the 3D regime in a continuum model.[87] In our simulations, we possibly cannot reach the late-stage Ostwald ripening, while the contribution of domain merging is also minor in the small monolayers. The crossover to $\alpha \approx {}^1/_2$ for the large monolayers could correspond to Brownian coagulation in 2D. On the other hand, a finite L_H comparable to the domain size could break the dynamical scaling in our systems. In addition, because of the limited length and time scales covered, our simulations possibly did not reach the asymptotic scaling regime.[96]

DISCUSSION

We have presented a molecular view of phase transformations in lipid monolayers. Two physiologically relevant cases were considered: the coexistence of LE and LC phases and the coexistence of Lo and Ld phases. Unlike previous works, our large-scale simulations with explicit solvent allowed the formation of multiple domains with diameters of tens of nanometers while retaining the chemical specificity of different lipid types. We obtained detailed information on domain properties and followed the changes in properties over a range of surface tensions, which to our knowledge has not been previously studied in simulations. This high spatial and temporal resolution data on nanoscale domains can complement experimental data and provide new insights into phase transitions in lipid membranes.

Interestingly, phase transformations in the two considered lipid mixtures proceeded via distinct mechanisms, namely, nucleation and spinodal decomposition, respectively. These mechanisms were determined by points within different regions (with respect to the binodal/spinodal curves) of the lipid phase diagram, set by the selected lipid composition, temperature, and surface tension. When these conditions were changed, different transformation mechanisms could be observed [e.g., lowering the temperature in the LC/LE mixture led to spinodal decomposition (results not shown)]. On the other hand, when the temperature of the Lo/Ld mixture was increased, the phase behavior of the monolayer changed from stable domains to transient compositional fluctuations. This change in phase behavior could indicate that the system was in the vicinity of a critical point.[21] However, the calculated line tension values at the Ld−Lo interface were relatively high and did not support the latter. In addition, the structures of the Ld and Lo phases differ substantially (e.g., the thicknesses differ by ∼0.6 nm in bilayers[46]).

The driving forces for phase separation were also different in the two simulated systems. Separation into the Lo and Ld phases was induced by preferential interactions between cholesterol and the saturated lipid, leading to their segregation and to exclusion of unsaturated lipids from the Lo phase. Formation of the LC domains from the LE phase was induced by monolayer lateral compression upon lowering of the surface tension. The latter had a condensing effect on the (high-melting-temperature) DPPC lipid, similar to lowering the temperature.

The presence of domains changed the monolayer viscoelastic properties. The monolayer surface viscosity increased in the presence of domains, in particular because of morphological changes (in the Lo/Ld coexistence). The areas per lipid in the LE and LC phases remained nearly constant while the average area decreased upon monolayer compression. Monolayer compression changes the composition of the phases, which in turn regulates the phase structure in addition to surface tension in homogeneous mixtures. Segregation of lipid components leads to spontaneous curvature of Lo domains at low surface tensions. The latter develops as the work against the surface tension to increase the monolayer area accompanying its bending becomes low. Monolayer compression also leads to a reduction in the line tension at both the LE−LC and Lo−Ld interfaces, which could lead to smaller (nanoscale, raftlike) domains[93] and could also explain the restructuring from micro- to nanodomains upon reduction of surface tension in lung surfactant.[12,97]

It is worth mentioning the limitations of our simulations. We considered relatively low surface tensions (1−30 mN/m), which are relevant for the function of lung surfactant.[98] The monolayer surface density is comparable to that of bilayers at surface tensions of 30−40 mN/m. Lipid molecules constituting the considered mixtures were parametrized in the MARTINI

model to reproduce the properties of pure bilayers in a selected interval of temperatures.[34,65] The phase transition temperatures differ somewhat from the experimental values,[36,42] and they demonstrate a weaker temperature dependence because of substitution of entropic interactions by enthalpic ones in the reduced degrees of freedom due to coarse graining. Therefore, the phase diagrams of the considered mixtures cannot be exactly mapped to experimental phase diagrams. Nevertheless, we believe that the trends observed in our simulations are generally valid and could explain the properties of monolayers with phase coexistence.

This work has focused on lipid monolayers under varying surface tension. Decreasing surface tension in monolayers can be translated to decreasing temperature in bilayers.[99] We therefore believe that our results are of interest for understanding the phase behavior in lipid membranes in general. The large length and time scales of our simulations provide a bridge towards the state-of-the-art techniques, including super-resolution microscopy, atomic force microscopy, and secondary-ion mass spectroscopy,[15,51−53] while combining compositional, structural, and dynamic information. The detailed information on domain properties can improve our understanding of the lipid−lipid interactions underlying lateral heterogeneity in biological membranes.

■ CONCLUSIONS

We simulated transformations into LC/LE and Lo/Ld phases in lipid monolayers in the MARTINI coarse-grained model, and characterized the properties of monolayers with coexisting phases under varying surface tension. Partial lipid areas and phase composition showed different dependences on surface tension in the two lipid mixtures. The domain boundary length increased and the line tension decreased with decreasing surface tension. The monolayer surface viscosity increased as a result of domain reorganization under shear. Domains of the Lo phase manifested spontaneous curvature at low surface tensions. The transformation from the mixed state to a separated state occurred via nucleation and growth in one case and spinodal decomposition in the second case, with distinct coarsening kinetics. These simulations provide new insight into both the structure and dynamics of monolayers with nanosized domains and represent a significant step towards an improved understanding of mixed biological monolayers and bilayers.

■ AUTHOR INFORMATION

Corresponding Author

tieleman@ucalgary.ca

Notes

The authors declare no competing financial interest.

■ ACKNOWLEDGMENTS

This work was supported by the Natural Sciences and Engineering Research Council (Canada) (S.B.) and the Canadian Institutes for Health Research (E.M.-V.). D.P.T. is an Alberta Innovates Health Solutions Scientist and Alberta Innovates Technology Futures Strategic Chair in (Bio) Molecular Simulation. The simulations were performed on Westgrid/Compute Canada facilities.

■ REFERENCES

(1) Mouritsen, O. G. *Life—As a Matter of Fat*; Springer: Berlin, 2005.
(2) Engelman, D. M. *Nature* **2005**, *438*, 578.
(3) van Meer, G.; Voelker, D. R.; Feigenson, G. W. *Nat. Rev. Mol. Cell Biol.* **2008**, *9*, 112.
(4) Lingwood, D.; Simons, K. *Science* **2010**, *327*, 46.
(5) Pike, L. J. *J. Lipid Res.* **2006**, *47*, 1597.
(6) Brown, D. A.; London, E. *Annu. Rev. Cell Dev. Biol.* **1998**, *14*, 111.
(7) Simons, K.; Ikonen, E. *Nature* **1997**, *387*, 569.
(8) Simons, K.; Toomre, D. *Nat. Rev. Mol. Cell Biol.* **2000**, *1*, 31.
(9) Mayor, S.; Rao, M. *Traffic* **2004**, *5*, 231.
(10) Parton, R. G.; Richards, A. A. *Traffic* **2003**, *4*, 724.
(11) Clements, J. A. *Am. Rev. Respir. Dis.* **1977**, *115*, 67.
(12) Nag, K.; Perez-Gil, J.; Ruano, M. L. F.; Worthman, L. A. D.; Stewart, J.; Casals, C.; Keough, K. M. W. *Biophys. J.* **1998**, *74*, 2983.
(13) Bernardino de la Serna, J.; Perez-Gil, J.; Simonsen, A. C.; Bagatolli, L. A. *J. Biol. Chem.* **2004**, *279*, 40715.
(14) Zuo, Y. Y.; Tadayyon, S. M.; Keating, E.; Zhao, L.; Veldhuizen, R. A. W.; Petersen, N. O.; Amrein, M. W.; Possmayer, F. *Biophys. J.* **2008**, *95*, 2779.
(15) Keating, E.; Zuo, Y. Y.; Tadayyon, S. M.; Petersen, N. O.; Possmayer, F.; Veldhuizen, R. A. W. *Biochim. Biophys. Acta* **2012**, *1818*, 1225.
(16) Leslie, M. *Science* **2011**, *334*, 1046.
(17) Fan, J.; Sammalkorpi, M.; Haataja, M. *FEBS Lett.* **2010**, *584*, 1678.
(18) Ziolkowska, N. E.; Christiano, R.; Walther, T. C. *Trends Cell. Biol.* **2012**, *22*, 151.
(19) Lenne, P.-F.; Nicolas, A. *Soft Matter* **2009**, *5*, 2841.
(20) Jacobson, K.; Mouritsen, O. G.; Anderson, R. G. W. *Nat. Cell Biol.* **2007**, *9*, 7.
(21) Honerkamp-Smith, A. R.; Veatch, S. L.; Keller, S. L. *Biochim. Biophys. Acta* **2009**, *1788*, 53.
(22) Veatch, S. L.; Soubias, O.; Keller, S. L.; Gawrisch, K. *Proc. Natl. Acad. Sci. U.S.A.* **2007**, *104*, 17650.
(23) Honerkamp-Smith, A. R.; Cicuta, P.; Collins, M. D.; Veatch, S. L.; den Nijs, M.; Schick, M.; Keller, S. L. *Biophys. J.* **2008**, *95*, 236.
(24) Collins, M. D.; Keller, S. L. *Proc. Natl. Acad. Sci. U.S.A.* **2008**, *105*, 124.
(25) Kiessling, V.; Crane, J. M.; Tamm, L. K. *Biophys. J.* **2006**, *91*, 3313.
(26) Schick, M. *Phys. Rev. E* **2012**, *85*, No. 031902.
(27) Brewster, R.; Pincus, P. A.; Safran, S. A. *Biophys. J.* **2009**, *97*, 1087.
(28) Brewster, R.; Safran, S. A. *Biophys. J.* **2010**, *98*, L21.
(29) Baumgart, T.; Hess, S. T.; Webb, W. W. *Nature* **2003**, *425*, 821.
(30) Semrau, S.; Schmidt, T. *Soft Matter* **2009**, *5*, 3174.
(31) McConnell, H. M.; Tamm, L. K.; Weis, R. M. *Proc. Natl. Acad. Sci. U.S.A.* **1984**, *81*, 3249.
(32) Travesset, A. *J. Chem. Phys.* **2006**, *125*, No. 084905.
(33) Elson, E. L.; Fried, E.; Dolbow, J. E.; Genin, G. M. *Annu. Rev. Biophys.* **2010**, *39*, 207.
(34) Marrink, S. J.; Risselada, H. J.; Yefimov, S.; Tieleman, D. P.; Vries, A. H. *J. Phys. Chem. B* **2007**, *111*, 7812.
(35) de Vries, A. H.; Yefimov, S.; Mark, A. E.; Marrink, S. J. *Proc. Natl. Acad. Sci. U.S.A.* **2005**, *102*, 5392.
(36) Marrink, S. J.; Risselada, J.; Mark, A. E. *Chem. Phys. Lipids* **2005**, *135*, 223.
(37) Mohammad-Aghaie, D.; Mace, E.; Sennoga, C. A.; Seddon, J. M.; Bresme, F. *J. Phys. Chem. B* **2010**, *114*, 1325.
(38) Duncan, S. L.; Larson, R. G. *Biophys. J.* **2008**, *94*, 2965.
(39) Stevens, M. J. *J. Chem. Phys.* **2004**, *121*, 11942.
(40) Rodgers, J. M.; Sorensen, J.; de Meyer, F. J. M.; Schiott, B.; Smit, B. *J. Phys. Chem. B* **2012**, *116*, 1551.
(41) Duncan, S. L.; Dalal, I. S.; Larson, R. G. *Biochim. Biophys. Acta* **2011**, *1808*, 2450.
(42) Baoukina, S.; Monticelli, L.; Marrink, S. J.; Tieleman, D. P. *Langmuir* **2007**, *23*, 12617.
(43) Faller, R.; Marrink, S. J. *Langmuir* **2004**, *20*, 7686.
(44) Hömberg, M.; Müller, M. *J. Chem. Phys.* **2010**, *132*, No. 155104.

(45) Muddana, H. S.; Chiang, H. H.; Butler, P. J. *Biophys. J.* **2012**, *102*, 489.
(46) Risselada, H. J.; Marrink, S. J. *Proc. Natl. Acad. Sci. U.S.A.* **2008**, *105*, 17367.
(47) Perlmutter, J. D.; Sachs, J. N. *J. Am. Chem. Soc.* **2011**, *133*, 6563.
(48) Domanski, J.; Marrink, S. J.; Schafer, L. V. *Biochim. Biophys. Acta* **2012**, *1818*, 984.
(49) Risselada, H. J.; Marrink, S. J.; Muller, M. *Phys. Rev. Lett.* **2011**, *106*, No. 148102.
(50) Schaefer, L. V.; de Jong, D. H.; Holt, A.; Rzepiela, A. J.; de Vries, A. H.; Poolman, B.; Killian, J. A.; Marrink, S. J. *Proc. Natl. Acad. Sci. U.S.A.* **2011**, *108*, 1343.
(51) Eggeling, C.; Ringemann, C.; Medda, R.; Schwarzmann, G.; Sandhoff, K.; Polyakova, S.; Belov, V. N.; Hein, B.; von Middendorff, C.; Schoenle, A.; Hell, S. W. *Nature* **2009**, *457*, 1159.
(52) Hess, S. T.; Gould, T. J.; Gudheti, M. V.; Maas, S. A.; Mills, K. D.; Zimmerberg, J. *Proc. Natl. Acad. Sci. U.S.A.* **2007**, *104*, 17370.
(53) Owen, D. M.; Rentero, C.; Rossy, J.; Magenau, A.; Williamson, D.; Rodriguez, M.; Gaus, K. *J. Biophotonics* **2010**, *3*, 446.
(54) Hess, B.; Kutzner, C.; van der Spoel, D.; Lindahl, E. *J. Chem. Theory Comput.* **2008**, *4*, 435.
(55) Baoukina, S.; Monticelli, L.; Amrein, M.; Tieleman, D. P. *Biophys. J.* **2007**, *93*, 3775.
(56) Baoukina, S.; Monticelli, L.; Risselada, H. J.; Marrink, S. J.; Tieleman, D. P. *Proc. Natl. Acad. Sci. U.S.A.* **2008**, *105*, 10803.
(57) Bussi, G.; Donadio, D.; Parrinello, M. *J. Chem. Phys.* **2007**, *126*, No. 014101.
(58) Berendsen, H. J. C.; Postma, J. P. M.; van Gunsteren, W. F.; DiNola, A.; Haak, J. R. *J. Chem. Phys.* **1984**, *81*, 3684.
(59) Goga, N.; Rzepiela, A. J.; de Vries, A. H.; Marrink, S. J.; Berendsen, H. J. C. *J. Chem. Theory Comput.* **2012**, DOI: 10.1021/ct3000876.
(60) den Otter, W. K.; Shkulipa, S. A. *Biophys. J.* **2007**, *93*, 423.
(61) Smaby, J. M.; Brockman, H. L.; Brown, R. E. *Biochemistry* **1994**, *33*, 9135.
(62) Sugar, I. P.; Chong, P. L. G. *J. Am. Chem. Soc.* **2012**, *134*, 1164.
(63) Ali, M. R.; Cheng, K. H.; Huang, J. *Proc. Natl. Acad. Sci. U.S.A.* **2007**, *104*, 5372.
(64) Veatch, S. L.; Polozov, I. V.; Gawrisch, K.; Keller, S. L. *Biophys. J.* **2004**, *86*, 2910.
(65) Marrink, S. J.; de Vries, A. H.; Mark, A. E. *J. Phys. Chem. B* **2004**, *108*, 750.
(66) Nagle, J. F.; Tristram-Nagle, S. *Biochim. Biophys. Acta* **2000**, *1469*, 159.
(67) Benvegnu, D. J.; McConnell, H. M. *J. Phys. Chem.* **1992**, *96*, 6820.
(68) Blanchette, C. D.; Lin, W.-C.; Orme, C. A.; Ratto, T. V.; Longo, M. L. *Langmuir* **2007**, *23*, 5875.
(69) Tian, A.; Johnson, C.; Wang, W.; Baumgart, T. *Phys. Rev. Lett.* **2007**, *98*, No. 208102.
(70) Stottrup, B. L.; Heussler, A. M.; Bibelnieks, T. A. *J. Phys. Chem. B* **2007**, *111*, 11091.
(71) Schafer, L. V.; Marrink, S. J. *Biophys. J.* **2010**, *99*, L91.
(72) Lee, B. S.; Mabry, S. A.; Jonas, A.; Jonas, J. *Chem. Phys. Lipids* **1995**, *78*, 103.
(73) Kuo, A. L.; Wade, C. G. *Biochemistry* **1979**, *18*, 2300.
(74) Filippov, A.; Oradd, G.; Lindblom, G. *Biophys. J.* **2006**, *90*, 2086.
(75) Kahya, N.; Scherfeld, D.; Bacia, K.; Poolman, B.; Schwille, P. *J. Biol. Chem.* **2003**, *278*, 28109.
(76) Wang, W.; Yang, L.; Huang, H. W. *Biophys. J.* **2007**, *92*, 2819.
(77) Cicuta, P.; Keller, S. L.; Veatch, S. L. *J. Phys. Chem. B* **2007**, *111*, 3328.
(78) Espinosa, G.; Lopez-Montero, I.; Monroy, F.; Langevin, D. *Proc. Natl. Acad. Sci. U.S.A.* **2011**, *108*, 6008.
(79) Wilke, N.; Vega Mercado, F.; Maggio, B. *Langmuir* **2010**, *26*, 11050.
(80) Bray, A. J. *Adv. Phys.* **2002**, *51*, 481.
(81) Gunton, J. D.; Miguel, M. S.; Sahni, P. S. *Phase Transitions and Critical Phenomena*; Academic Press: New York, 1983; Vol. *8*.
(82) Hohenberg, P. C.; Halperin, B. I. *Rev. Mod. Phys.* **1977**, *49*, 435.
(83) Elder, K. R.; Morin, B.; Grant, M.; Desai, R. C. *Phys. Rev. B* **1991**, *44*, 6673.
(84) Ehrig, J.; Petrov, E. P.; Schwille, P. *New J. Phys.* **2011**, *13*, No. 045019.
(85) Haataja, M. *Phys. Rev. E* **2009**, *80*, No. 020902.
(86) Fan, J.; Han, T.; Haataja, M. *J. Chem. Phys.* **2010**, *133*, No. 235101.
(87) Camley, B. A.; Brown, F. L. H. *J. Chem. Phys.* **2011**, *135*, No. 225106.
(88) Siggia, E. D. *Phys. Rev. A* **1979**, *20*, 595.
(89) Miguel, M. S.; Grant, M.; Gunton, J. D. *Phys. Rev. A* **1985**, *31*, 1001.
(90) Camley, B. A.; Brown, F. L. H. *Phys. Rev. Lett.* **2010**, *105*, No. 148102.
(91) Laradji, M.; Kumar, P. B. S. *J. Chem. Phys.* **2005**, *123*, No. 224902.
(92) Lifshitz, I. M.; Slyozov, V. V. *J. Phys. Chem. Solids* **1961**, *19*, 35.
(93) Frolov, V. A. J.; Chizmadzhev, Y. A.; Cohen, F. S.; Zimmerberg, J. *Biophys. J.* **2006**, *91*, 189.
(94) Binder, K.; Stauffer, D. *Phys. Rev. Lett.* **1974**, *33*, 1006.
(95) Ramachandran, S.; Komura, S.; Gompper, G. *EPL* **2010**, *89*, No. 56001.
(96) Grant, M.; Elder, K. R. *Phys. Rev. Lett.* **1999**, *82*, 14.
(97) Zuo, Y. Y.; Keating, E.; Zhao, L.; Tadayyon, S. M.; Veldhuizen, R. A. W.; Petersen, N. O.; Possmayer, F. *Biophys. J.* **2008**, *94*, 3549.
(98) Bachofen, H.; Schurch, S. *Comp. Biochem. Physiol., Part A: Mol. Integr. Physiol.* **2001**, *129*, 183.
(99) Stottrup, B. L.; Stevens, D. S.; Keller, S. L. *Biophys. J.* **2005**, *88*, 269.